Inorganic Chemistry

Article

pubs.acs.org/IC

Electronic Structure of One-Electron-Oxidized Form of the Methylcobalamin Cofactor: Spin Density Distribution and Pseudo-Jahn−Teller Effect

Neeraj Kumar,[†] Jadwiga Kuta,[†] Wlodzimierz Galezowski,[‡] and Pawel M. Kozlowski*,[†]

[†]Department of Chemistry, University of Louisville, Louisville, Kentucky 40292, United States

[‡]Department of Chemistry, A. Mickiewicz University, Umultowska 89b, 61-614 Poznan, Poland

Supporting Information

ABSTRACT: The electronic and structural properties of the one-electron-oxidized form of methylcobalamin (MeCbl) cofactor have been investigated using density functional theory (DFT) and CASSCF/MC-XQDPT2 calculations. We applied two types of functionals (hybrid and GGA) which produced quite different results in terms of spin density profiles: the B3LYP description was consistent with Co(III) and the π-cation corrin radical while the BP86 result was more in line with the Co(IV) oxidation state. A closer inspection of both outcomes indicates that the oxidized species have a mixed π-cation corrin radical and Co(III)/Co(IV) character. This mixed character was further supported by high-level *ab initio* CASSCF/MC-XQDPT2 calculations, which reveal the strong mixing of the electronic states due to nondynamical correlation effects. The near degeneracy, which takes place between the ground and first excited state, was consistent with the presence of a pseudo-Jahn−Teller (pJT) effect in the oxidized form of MeCbl. In addition, the DFT-based investigation of the structurally related porphyrin complexes gives a description consistent with corrin-based analogues and reveals that the corrin species have more Co(IV) character. The most important finding of the present study, regardless of the type of functional used, was the significant lowering of dissociation energy (~35%), which might be due to the partial depopulation of the Co−C σ orbital upon removal of an electron.

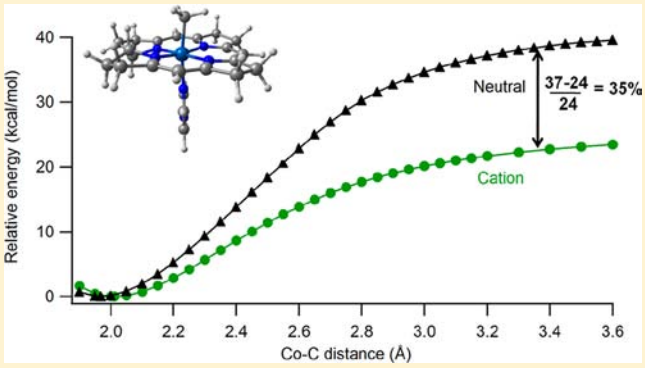

1. INTRODUCTION

Methylcobalamin (MeCbl, Figure 1) is the cofactor of several methyltransferases such as methionine synthase (MetH) or enzymes that participate in the carbon dioxide fixation pathway.[1−5] The enzymatic mechanisms for the methyl transfer require the cleavage and the formation of a Co−C bond in the presence of an additional cofactor, either a Zn^{2+} ion or a $[Fe_4S_4]$ cluster.[6,7] In solution, MeCbl is a very sluggish catalyst in contrast to an enzyme-bound MeCbl where transfer of the methyl group is very efficient.[8−13] The methyl transfer mechanism has been commonly interpreted as an S_N2-type nucleophilic displacement; however, other proposals including one-electron reduction or oxidation of cobalt corrinoids[14] were also considered. The Co−C bond cleavage in the one-electron-reduced (1e-Red) form of the cobalt corrinoids[9−13] has attained a considerable amount of interest because the Co−C bond dissociation energy (BDE) is significantly decreased. The 1e-Red B_{12} cofactors[9−13] (Figure 1) and related model complexes[15−21] have been investigated experimentally as well as computationally to explore the reductive cleavage mechanism.[22−24] For the MeCbl cofactor[22,24] (Figure 1), it has been found using density functional theory (DFT) that the addition of an electron results in the formation of a π-corrin radical anion. Subsequently, when the Co−C bond was stretched, the

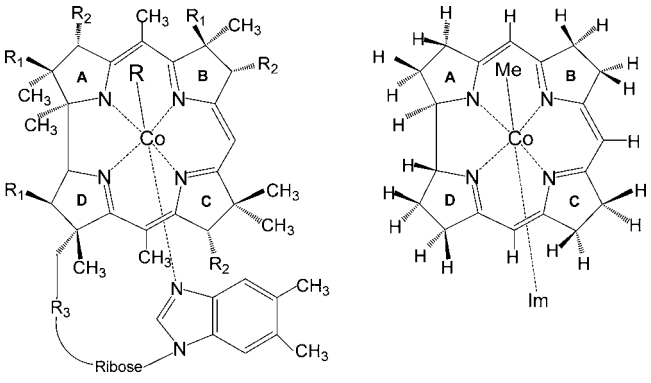

Figure 1. Molecular structure of B_{12} cofactors (left panel) where R = Me for MeCbl and R = Ado for AdoCbl (R_1 = CH_2CONH_2, R_2 = $CH_2CH_2CONH_2$, R_3 = $(CH_2)_2CONHCH_2CH(CH_3)OPO_3^-$). The right panel shows the structural model of MeCbl employed in the present study and denoted as Im-[Co^{III}(corrin)]-Me^+.

Received: June 25, 2012
Published: January 29, 2013

   dx.doi.org/10.1021/ic3013443 | *Inorg. Chem.* 2013, 52, 1762−1771

electron shifted from the corrin-based π^* to bond-centered σ^*_{Co-C} orbital, which results in the cleavage of the three-electron $(\sigma)^2(\sigma^*)^1$ bond.[22] A similar DFT analysis of the Co−C bond cleavage in the neutral as well as in the 1e-Red form of alkyl-cobalt(III) phthalocyanines[23] confirmed the validity of the reductive cleavage mechanism proposed for the MeCbl.[22,24]

Despite the fact that the oxidative mechanism was considered a long time ago as one of the possible routes for alkyl transfer from alkylcobalamins,[25] the Co−C bond cleavage of one-electron-oxidized (1e-Ox) cobalt corrinoids has gained less attention compared to the reductive cleavage. The electronic and structural properties of species generated upon oxidation remain unexplored, mainly because these species are unstable and difficult to characterize experimentally.[26] The alkylcobalt(IV) complexes with various equatorial ligands can be studied only at low temperatures.[27] It is noteworthy that a quite rapid Co−C bond cleavage was observed during electrochemical oxidation of MeCbl in aqueous solution with aquoCo(III)-cobalamin and methanol as the final products.[28] It has been further suggested that one-electron oxidation leads to depopulation of the Co−C σ orbital, which consequently would reduce the bond strength.[28] The resulting species then would have d^5 cobalt(IV) character, and the BDE of the Co(IV)−C bond should be significantly lower in comparison to Co(III)−C. As an alternative to the Co(IV) state, the corrin ligand could be oxidized leading to a corrin−based radical in analogy to the heme-containing systems where usually the porphyrin ligand is oxidized.[29,30]

Initially, the formation of Co(IV)−C and π-cation radicals with Co(III)−C species in 1e-Ox organocobalt complexes had been thoroughly investigated by Halpern et al.,[31,32] where they distinguished these two electronic species using the super-hyperfine structure of the EPR spectrum.[33] It was demonstrated for 1e-Ox methylcobaloximes[34] that the odd electron resides mainly on the cobalt d orbital which is not directed toward the donor N atoms, thus giving a dominant contribution to the singly occupied molecular orbital (SOMO), with a small contribution from the cobalt $4p_z$ orbital.[33] A similar location of the unpaired electron was also suggested for the 1e-Ox alkylcobaltporphyrin.[35] Although these studies established that the 1e-Ox alkylcobalt complexes are usually formulated as Co(IV) species,[26] it was further put into question if the oxidized organocobalt porphyrins (which are structurally related to corrinoids) should be described as the ligand centered π-cation radicals Co(III) rather than the Co(IV) species.[19,36] On the other hand, the electronic properties of the organocobalt porphyrins[36] imply that the 1e-Ox cobalt corrinoids may have mixed π-cation corrin radical and Co(III)/Co(IV) character.

Almost two decades later, Fukuzumi et al. pointed out such dichotomy for organocobalt tetraphenylporphyrins, [B-(TPP)-Co-R]$^+$, where they studied the role of different axial ligands.[35] They observed that the oxidized species for both R = Me and phenyl have a Co(III) π-cation radical character in dichloromethane (with no respectable B), but in weakly binding acetonitrile, the [MeCN-(TPP)Co-Me]$^+$ species has more Co(IV) character than its [MeCN-(TPP)Co-Ph]$^+$ analogue. Additionally, with a stronger axial base (B), pyridine, both complexes have a dominant Co(IV) character. Furthermore, it has been suggested that the homolytic cleavage of the Co−C bond in the Co(IV) complexes is easier than in the π-cation radicals with Co(III).[35] The formation of Co(IV) species in oxidized coenzyme B_{12} model complexes, i.e., cobaloximes, [B-$Co^{IV}(DH)_2$-R]$^+$ and subsequent Co(IV)−C bond cleavage have been further observed by Fukuzumi and Ohkubo,[37] wherein they revealed that regardless of the mechanism, the Co−C bond cleavage is facilitated by the presence of an axial base. Alternatively, Fanchiang et al.[38] proposed that the 1e-Ox MeCbl species is involved in the methyl transfer between MeCbl and diaquo-Co(III)cobinamide. It was suggested that within a bimolecular complex, the diaquo-Co(III)cobinamide form of the cofactor oxidizes MeCbl and subsequently forms Co(II)cobinamide, which serves as a methyl acceptor.[38] This particular methyl transfer reaction demonstrates that the oxidative cleavage of the Co−C bond might have relevance to the enzymatic catalysis. In addition, it has been investigated using kinetic measurements of various reactions between the methylcobalamin and oxidizing agents such as $AuCl_4^-$, $IrCl_6^{2-}$, and Fe^{3+} ions that a single electron transfer from MeCbl to these oxidants is feasible which initiates the cleavage of the Co−C bond.[39−43] These experimental findings are more in line with oxidative cleavage mechanism of the Co−C bond.

The coordination state is very important for the chemistry of corrinoids to understand the efficient cleavage of the Co−C bond. The MeCbl cofactor has a dimethylbenzimidazole (DBI) axial base coordinated to the cobalt in solution (except for acidic conditions) as well as in the enzymatic environment where this intramolecular base is replaced by a histidine residue from the protein.[44] Since the MeCbl cofactor preferably exists as a six-coordinate 18-electron species, its 1e-Ox analogue must show even stronger demand for an axial base. This is the reason why the Co−C bond cleavage in the 1e-Red species involves a five-coordinate base-off form, as it was concluded in the recent DFT study,[22,24] while the 1e-Ox form requires a base at the lower axial position.

On the basis of the previous studies, one can conclude that the electronic structure of the 1e-Ox cobalt corrinoids is a subject of debate, because the exact location of the unpaired electron remains elusive. Herein, we employed two different types of computational tools to analyze the electronic and structural properties of the 1e-Ox MeCbl. We applied a DFT for the 1e-Ox MeCbl and its related metalloporphyrins in order to gain insight into the Co−C bond properties. Subsequently, the time-dependent DFT (TD-DFT) calculations were carried out to investigate the nature of low-lying excited states and validate the oxidative cleavage mechanism. The complex electronic structure of the 1e-Ox MeCbl revealed by the DFT was further analyzed using the CASSCF/MC-XQDPT2 calculations. A particular emphasis was placed on the Co−C bond cleavage in the 1e-Ox form of MeCbl and the relevant mechanism responsible for the lowering of the dissociation energy as compared to its neutral analogue.

2. COMPUTATIONAL DETAILS

2.1. Structural Models. A simplified model of MeCbl, denoted as Im-[Co^{III}(corrin)]-Me^+ (Figure 1, right panel), has been employed where all the amide side chains were replaced with hydrogen atoms, and the lower axial ligand was modeled with the imidazole (Im) moiety. These types of truncated models have been extensively used in previous studies, with success, to predict the electronic and structural properties of B_{12} cofactors.[45−47] Consequently, the truncated model of MeCbl has been used to generate 1e-Ox MeCbl species. In order to gain further insight into the Co−C bond properties of the 1e-Ox MeCbl species, we have also utilized structurally related porphine-based complexes, B-[Co^{III}(Por)]-Me with pyridine or imidazole as an axial base (B). The relevant geometrical parameters as well as Cartesian coordinates used for all optimized structures employed in

dx.doi.org/10.1021/ic3013443 | Inorg. Chem. 2013, 52, 1762−1771

Table 1. Relevant Co−C BDEs (kcal/mol) and Axial Bond Lengths (Å) of the Neutral, 1e-Ox, and 1e-Red MeCbl Models Computed at the BP86/6-31G* and B3LYP/6-31G* Levels of Theory

	experiment	BP86			B3LYP	
parameter	neutral	neutral	1e-Ox	1e-Red	neutral	1e-Ox
Co−C	1.979[62]	1.968	2.011	1.958	1.956	2.031
Co−N_{ax}	2.162[62]	2.132	2.063	2.112	2.179	2.050
BDE[a]	37(3)[65]	37.0	24.2	20.4[b]	24.1	16.1[b]
BDE lowering (%)			35	45		33

[a]ZPE corrected. [b]BDE of the base-off species.

the present work can be found in the Supporting Information (Tables S1−S6).

2.2. DFT Calculations. The DFT method has been used due to its effectiveness in the investigation of the electronic and structural properties of the alkyl-cobalt(III) complexes, including cobalt corrinoids.[45−49] The use of a suitable functional is important for the accurate prediction of the Co−C bond dissociation energy. Thus, the geometry optimization of all models as well as electronic structure calculations has been carried out using the BP86[50,51] functional and the 6-31G(d) (5d components) basis set, as implemented in Gaussian 03.[52] It has been pointed out for the 1e-Ox nitrosyl cobaltporphyrin that the B3LYP functional gives spin density distribution which is similar to the experimental data as compared to the BP86 functional.[53] In addition, it has been demonstrated recently that the spin polarized solution of cob(I)alamin complexes[54,55] cannot be obtained with pure GGA functionals such as PBE[56] because they fail to converge to a spin polarized solution at the ground state singlet. Despite the fact that the hybrid B3LYP functional underestimates the strength of the Co−C bond due to the presence of HF exchange,[57] it is appropriate for the prediction of a broken symmetry solution.[58] Therefore, we applied the B3LYP functional as well for all models.[59]

2.3. CASSCF/MC-XQDPT2 Calculations. The DFT computations, which are based on the Kohn−Sham formalism, cannot describe the multiconfigurational character as well as near-degeneracy problems of the electronic states of the MeCbl model system because they are restricted to a single Slater determinant description. Thus, we performed multireference CASSCF calculations, followed by quasi-degenerate perturbation theory (QDPT2)[60] calculations with a multiconfigurational self-consistent-field reference function (MC-XQDPT2) to include the dynamical correlation, as implemented in the PC GAMESS/Firefly QC package.[61] The CASSCF calculations were carried out on the DFT optimized structure of the 1e-Ox MeCbl model using the 6-31G(d) basis set.

3. RESULTS AND DISCUSSION

3.1. Geometry of the 1e-Ox Form of MeCbl and Related Porphine Complexes. At first, the previously used structural model of MeCbl, i.e., Im-[Co^{III}(corrin)]-Me^+, was optimized employing BP86 and B3LYP functionals. The fact that this level of theory (DFT) provides axial bond lengths comparable with X-ray data[62] (Table 1) strengthens our confidence that the structure of 1e-Ox MeCbl species would also be well described with these functionals. The optimization of the 1e-Ox MeCbl reveals that its key geometrical parameters are not significantly different from those of the parent complex. The removal of an electron has small influence on axial bond lengths; the Co−C bond elongates from 1.968 to 2.011 Å while the Co−N_{Im} bond contracts from 2.132 to 2.063 Å (Table 1) as noticed with the BP86 functional. A similar trend of elongation and shortening of the axial bonds was also observed with the B3LYP functional. Furthermore, a very small change of the corrin structure was obtained because the corrin ring is very robust and not influenced by the nature of the axial ligand. It is important to mention that these changes in axial bond lengths of the 1e-Ox MeCbl are more pronounced than that of the 1e-Red MeCbl species where the single electron is mainly located on the corrin ring. Although the modulation of axial bond lengths seems to be consistent with some Co(IV) character of the 1e-Ox MeCbl, the bond lengthening is not substantial enough to signify the complete removal of an electron from the Co−C σ bond. The ∼0.05 Å longer Co−C bond in 1e-Ox species than in the 1e-Red MeCbl goes somehow against chemical intuition (shorter bonds are usually stronger), as the latter complex has a lower Co−C BDE (Table 1). This can be further explained in terms of the coordination of the lower axial base.

Due to the lack of extensive experimental data of the 1e-Ox MeCbl species, we employed structurally related porphyrin-based complexes, B-[Co^{III}(Por)]-Me (Figure 4), for DFT calculations as they are typically used in experimental studies with different bases B (pyridine or imidazole).[35] Moreover, it would also be interesting to see if any specific features of the corrin ligand, important for the Co−C bond cleavage in the 1e-Ox species, could be identified in comparison with the porphine complexes. The optimized Co−C bond of porphyrins is a few hundredths of an Ångstrom shorter than that observed for the corrin model (Table 2). The axial bond distances obtained with the BP86 functional are also shorter than the corresponding B3LYP values, as observed for the 1e-Ox MeCbl. This is mainly due to the difference in the metal−ligand bond covalency predicted by these two functionals. However, the symmetry of the axial system is lower in the BP86 than B3LYP structure because in BP86 the C−Co−N_B angle is ∼170°, while it is close to 180° in the B3LYP optimized structure. In addition, the porphine ligand shows saddling which is considerably more extensive in the BP86 than the B3LYP optimized structures of the 1e-Ox B-[Co^{III}(Por)]-Me. This type of structural difference is absent in the 1e-Ox MeCbl where the geometry of corrin is virtually insensitive to the type of functional used.

Table 2. Relevant Geometrical Parameters of the 1e-Ox B-[Co^{III}(Por)]-Me (B = Im or Pyr) Optimized at the BP86/6-31G* and B3LYP/6-31G* Levels of Theory

axial base (B)	functional	Co−C (Å)	Co−N_B (Å)	C−Co−N_B(deg)
Im	BP86	1.989	2.050	170.5
Im	B3LYP	1.992	2.063	178.4
Pyr	BP86	1.951	2.088	171.1
Pyr	B3LYP	1.991	2.108	178.8

3.2. Electronic Structure of the 1e-Ox MeCbl. To investigate the electronic structure of the 1e-Ox species, the Kohn−Sham orbitals located near the HOMO−LUMO gap were extracted from the DFT calculations. The energy levels as well as the location of MOs essential for the Co−C bond rupture are shown in Figure 2. Within the simple three-orbital framework,[63] the so-called strain orbital

dx.doi.org/10.1021/ic3013443 | Inorg. Chem. 2013, 52, 1762−1771

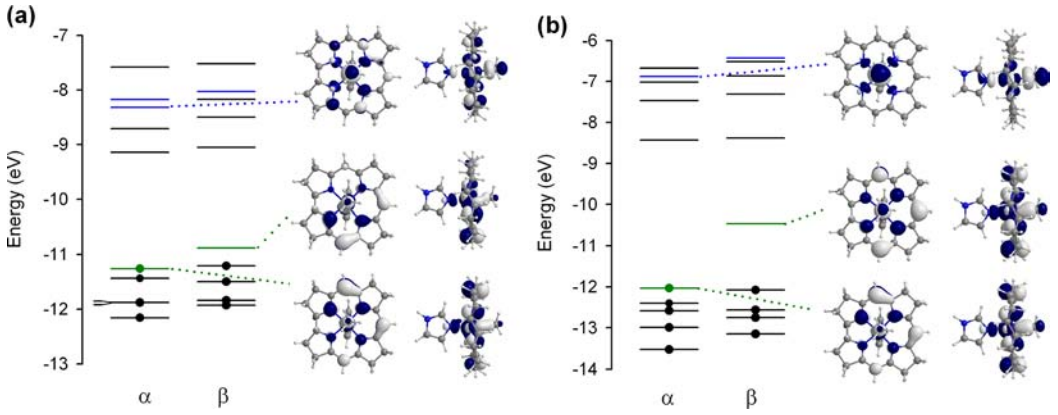

Figure 2. Orbital energy level diagram for 1e-Ox MeCbl: (a) BP86/6-31G* level of theory and (b) B3LYP/6-31G* level of theory. SOMO is indicated in green; the σ^* energy level is indicated in blue.

$$\sigma_{Co-C} \approx -c_1\phi[N(p_z)] + c_2\phi[Co(d_{z^2})] + c_3\phi[C(p_z)] \quad (1)$$

is of particular importance for predicting the properties of alkylcobalt complexes. This orbital has Co−C bonding character but is antibonding with respect to cobalt and nitrogen. In tetrapyrrole complexes, there is an interaction of this orbital with the π HOMO of the ligand. The ligand HOMO bears a resemblance to the a_{2u} orbital of the porphine dianion of D_{4h} symmetry and has large contributions not only from the p_z pyrrole nitrogen but also from the p_z orbitals of the bridging carbon atoms.

The SOMO shown in Figure 2 is the antibonding combination of an energetically higher a_{2u}-like π orbital of the equatorial ligand and a small contribution from the lower energetically lying σ_{Co-C}. Thus, the SOMO orbital has only weak Co−C bonding character:

$$SOMO \approx \phi[\phi_{corrin}] - \sigma_{Co-C} \quad (2)$$

The bonding combination of σ_{Co-C} and the π-ligand orbital has a large contribution from the σ_{Co-C}. This orbital, HOMO-4 for B3LYP in Figure 2b, and HOMO-6 and HOMO-7 for BP86, is ∼1.5 eV lower in energy than the SOMO (see Tables S7−S10 in the Supporting Information). Another orbital resulting from the three-orbital approach, depicted in Figure 2, is the higher energy antibonding σ of the Co−C bond (σ_{Co-C}^*). This orbital has double antibonding character because it is antibonding with respect to cobalt and nitrogen as well as with respect to cobalt and carbon (eq 3) and is energetically too far from the HOMO to play an important role in the Co−C bond cleavage in 1e-Ox methyl-cobalt species.

$$\sigma_{Co-C}^* \approx -c_1\phi[N(p_z)] + c_2\phi[Co(d_{z^2})] - c_3\phi[C(p_z)] \quad (3)$$

The orbital energies and the composition of most important molecular orbitals from BP86 and B3LYP calculations are shown in Tables S7−S10. Both functionals give a very similar picture of the SOMO orbital with respect to corrin as well as imidazole axial base contributions placing them at 72% (corrin) and 11% (Im) based on BP86, and 73% (corrin) and 9% (Im) according to B3LYP (Table 3). Nevertheless, the involvement of carbon and cobalt in the SOMO orbital is predicted to be somewhat different: BP86 gives more Co character (12%) and less carbon (4%), while the prediction based on the B3LYP is opposite, with a smaller contribution coming from cobalt (7%) and larger from carbon (9%).

Table 3. Composition of SOMO Molecular Orbital (in %) of the 1e-Ox MeCbl Determined at the BP86/6-31G* and B3LYP/6-31G* Levels of Theory

functional	C	Co	CH_3	Im	corrin
BP86	4	12	5	11	72
B3LYP	9	7	10	9	73

The composition of the SOMO (Table 3) indicates that the 1e-Ox complex does not have a true one electron Co−C bond. The bonding electron pair in the low-energy bonding combination of σ_{Co-C} (eq 1) and the a_{2u}-like orbital remains intact in the equilibrium structure of the 1e-Ox Im-[Co^{III}(corrin)]-Me^+ or its porphine 1e-Ox B-[Co^{III}(Por)]-Me analogues. Some depletion of the electron density from Co and the methyl group results from the absence of a β electron in the HOMO, but this orbital has only a marginal contribution to the Co−C bonding. Therefore, the Co−C bond elongation in the equilibrium structure of the 1e-Ox system is moderate. The spin density distributions in 1e-Ox B-[Co^{III}(Por)]-Me (B = Im or Pyr), which are similar to that of the 1e-Ox Im-[Co^{III}(corrin)]-Me^+, suggest that the SOMO in these species can also be described as an antibonding combination of an a_{2u}-like porphine π orbital and σ_{Co-C} (eq 2).

3.3. Spin Density Profiles in the 1e-Ox Models of MeCbl and Related Porphine Complexes. In the optimized structures of the 1e-Ox models, the unpaired electron is mainly distributed between cobalt and the corrin, or porphine, moiety (Figures 3, 4, and 5). The α spin density of the macrocycle is delocalized at the *meso* carbons as well as at the pyrrole nitrogens. Furthermore, the extent of spin distribution depends on the functional: spin density is evenly distributed between Co and corrin in the case of BP86, while it shifts more toward the corrin ring in the case of B3LYP. However, it turns out that the spin density on cobalt is not controlled by the SOMO in BP86-based optimized models of MeCbl as well as in its porphine analogues. The BP86 computed total spin densities on cobalt: 39% in the 1e-Ox Im-[Co^{III}(corrin)]-Me^+ or 43% and 44% in the 1e-Ox B-[Co^{III}(Por)]-Me^+ (B = Pyr or Im), respectively, are larger than the composition of the SOMOs (Table 3). This is noticeably a case of spin polarization, which usually emerged in DFT calculations of the electronic structures of paramagnetic metal complexes with red-ox active ligands.[64] The spin polarization occurs when at a given molecule spin contributions from α and β electrons, excluding the one residing in the SOMO, do not cancel. Indeed, the close examination of

dx.doi.org/10.1021/ic3013443 | Inorg. Chem. 2013, 52, 1762−1771

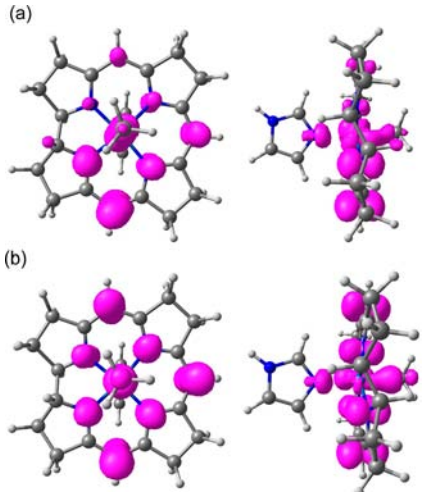

Figure 3. Spin density for the 1e-Ox MeCbl: (a) BP86/6-31G* level of theory and (b) B3LYP/6-31G* level of theory.

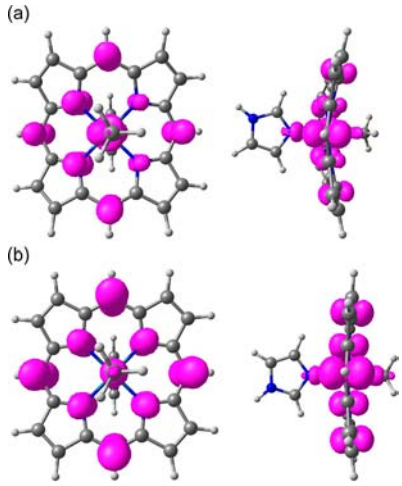

Figure 4. Spin density for the 1e-Ox Im-[Co^{III}(Por)]$^{\bullet}$-Me^{+}: (a) BP86/6-31G* level of theory and (b) B3LYP/6-31G* level of theory.

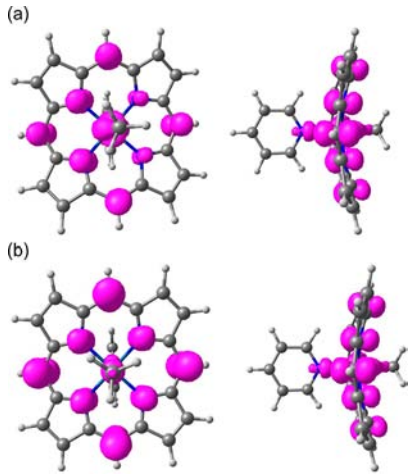

Figure 5. Spin density for the 1e-Ox Pyr-[Co^{III}(Por)]$^{\bullet}$-Me^{+}: (a) BP86/6-31G* level of theory and (b) B3LYP/6-31G* level of theory.

unrestricted orbitals (Figures S1 and S2) shows that the spatial parts of matching α and β electrons differ significantly from each other (see also Tables S7−S10 with composition of the orbitals). The spin polarization accumulates β spin on the corrin and α spin on the cobalt. As a result, net α spin density over the corrin is reduced and subsequently transferred to cobalt. On the other hand, the B3LYP calculations of the above-discussed model systems give α spin density of 7%, 5%, and 5%, respectively, on cobalt and 77%, 87%, and 86% over their equatorial ligands; therefore the spin polarization is small, which means that the SOMO describes correctly the spin delocalization.

We believe that the spin polarization has little connection with the formal oxidation state of the metal; i.e., both functionals show the 1e-Ox species as a prevalently Co(III) ligand π radical, with some admixture of the Co(IV) character. In the case of a strong spin polarization, the charge on cobalt is probably more reliable than spin density. The BP86 calculated Mulliken charge on the cobalt is +0.613 for 1e-Ox MeCbl, which is marginally larger than +0.559 of its neutral analogue. Because the B3LYP functional puts more emphasis on the ionic character of the bond due to inclusion of HF exchange, the computed charges are a bit larger (i.e, +0.696 and +0.629, respectively), but the difference caused by one-electron oxidation is similar to BP86, consistent with a small admixture of the d^5 Co(IV) state. Regardless of the methodology, the electronic charges of the metal in coordination compounds are much different from the formal oxidation states of the metal. However, the trends in atomic charges still reflect the change in the formal oxidation state of the metal in MeCbl, especially since the coordination state of the cobalt remains unchanged.

3.4. Dissociation of the Co−C Bond in the 1e-Ox MeCbl. The Co−C bond dissociation energy (BDE) computed as the energy difference between the fully optimized structure of Im-[Co^{III}(corrin)]-Me^{+} and its separate fragments, i.e., Im-[Co^{II}(corrin)]$^{+}$ and the methyl radical, gives a reliable estimation of the Co−C bond strength. The computed BDE with the BP86 for the neutral cofactor has a value of 42.0 kcal/mol, while zero point energy (ZPE) correction is equal to 5.0 kcal/mol. The ZPE corrected dissociation energy, i.e., 37.0 kcal/mol (see Table 1), is thus in excellent agreement with experimental values for the MeCbl of 37 ± 3 based on thermolysis[65] and 36 ± 4 kcal/mol employing calorimetric measurements,[66] respectively. On the other hand, the B3LYP functional, which is known to underestimate BDE,[22,49,67,68] gives a lower value of 29.5 kcal/mol, and after subtracting a ZPE correction, i.e., 5.4 kcal/mol, this value further decreases to 24.1 kcal/mol.

To analyze the cobalt−carbon bond dissociation in the 1e-Ox MeCbl model, the geometry optimization was first carried out along the Co−C stretch to verify that the Im-[Co^{III}(corrin)]$^{\bullet}$-Me^{2+} complex can dissociate properly. It was assumed that the cleavage is homolytic and leads to the formation of the methyl radical. The energy optimization along the Co−C coordinate produces a smooth dissociation curve with significant lowering in energy as compared to the neutral MeCbl (Figure 6). The cleavage of the Co−C bond was further explored by analysis of the low-lying excited states in addition to the ground state (Figures 7 and 8). The potential energy curves representing the lowest electronic excited states do not show any state crossing for either of the functionals, which indicates that the cleavage event involves only one electronic state in contrast to the 1e-Red species.[22] The accurate estimation of the Co−C BDE in the 1e-Ox model of MeCbl can be obtained as the energy difference between the full complex and its fragments according to the equation:

dx.doi.org/10.1021/ic3013443 | Inorg. Chem. 2013, 52, 1762−1771

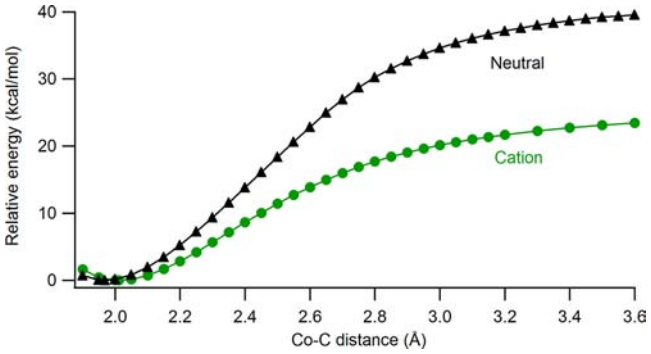

Figure 6. Comparison of dissociation curves for neutral and 1e-Ox forms of MeCbl calculated using the BP86/6-31G* level of theory.

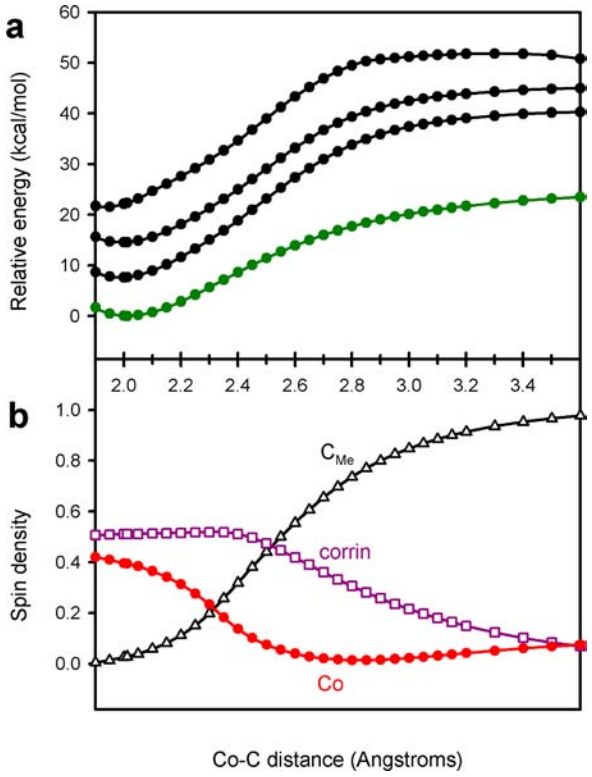

Figure 7. BP86/6-31G* calculated: (a) the ground state and low-lying electronic excited states for 1e-Ox MeCbl as a function of Co−C bond length and (b) spin density changes along the Co−C bond length.

$$\mathrm{Im{-}[Co^{III}(corrin)]^{\bullet}{-}Me^{2+}} \rightarrow \mathrm{Im{-}[Co^{III}(corrin)]^{2+}} + {}^{\bullet}\mathrm{Me} \quad (4)$$

The Co−C BDE determined using the BP86 functional is 24.2 kcal/mol after the ZPE correction (Table 1), while B3LYP leads to a much lower value of 16.1 kcal/mol as expected. Interestingly, the relative bond strength reduction in 1e-Ox models, computed as $(E_{1e\text{-}Ox} - E_{neutral})/E_{neutral}$, is essentially the same in both cases, i.e., 35% for BP86 and 33% for B3LYP. Although the absolute values are quite different, the relative changes appear independent of the type of functional used. We note that one electron reduction is more effective than one electron oxidation in weakening the Co−C bond.

The most noticeable structural change that takes place upon oxidative cleavage occurs in the Co−N_{Im} length, which is considerably shorter in Im-$[Co^{III}(corrin)]^{2+}$ because the antibonding character of orbitals involved in Co−N_{Im} is diminished (see eq 3). A similar change in Co−N_{ax} bond length takes place in the neutral cofactor upon heterolytic cleavage of the Co−C bond, as was predicted by the previous DFT analysis.[22] In both the neutral and the 1e-Ox species, the decreasing Co−N_{ax} distance with the Co−C stretch agrees with the observation that the presence of an axial base facilitates the homolytic Co−C bond cleavage.

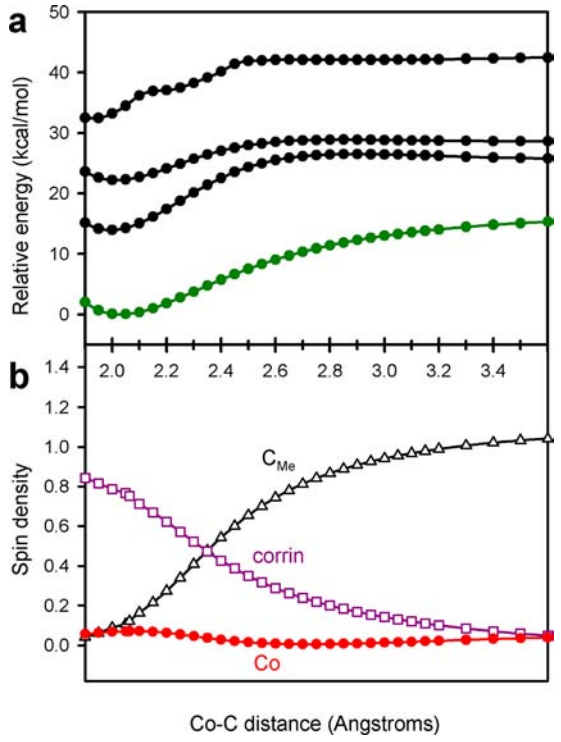

Figure 8. B3LYP/6-31G* calculated: (a) the ground state and low-lying electronic excited states for 1e-Ox MeCbl as a function of Co−C bond length and (b) spin density changes along the Co−C bond length.

3.5. Spin Density Changes along the Co−C Bond Stretch. The homolytic Co−C bond cleavage in the 1e-Ox model of MeCbl is associated with an intramolecular electron transfer from the Co−C bond onto the corrin cation radical. The analysis of the spin density changes provides further insight into the oxidative cleavage mechanism, particularly because these modulations are associated with the ground state properties, and can be accurately described by the DFT computations. The changes of the spin density associated with the corrin ring, cobalt, and the methyl carbon caused by the Co−C bond elongation were extracted from the DFT calculations and plotted together with the potential energy curves as shown in Figures 7 and 8 (lower panels), while the contours of the spin density for various Co−C bond lengths are shown in Figures S3 and S4 (Supporting Information). It is important to mention that the changes predicted on the basis of the B3LYP and BP86 functionals are rather different. The B3LYP functional describes the 1e-Ox species as essentially Co(III) and the ligand π radical, with small spin polarization (defined as the differences of α and β spin densities for Co and the corrin as a whole, with the exclusion of the contributions from the SOMO). The modulations in spin distribution between the equatorial ligand, cobalt, and methyl along the Co−C stretch (Figure 8) give a straightforward description of

dx.doi.org/10.1021/ic3013443 | Inorg. Chem. 2013, 52, 1762−1771

the bond cleavage: the β electron of the Co−C bonding pair shifts to corrin via cobalt, which behaves as a conductor. As a result, the α-spin at the methyl increases while the α-spin over the equatorial ligand disappears. This clear description of the Co−C bond is rather lost in the case of the BP86 functional due to a spin polarization. The BP86 calculated α spin density on corrin remains unchanged until the Co−C bond is stretched to ∼2.4 Å (Figure 7), and then it shifts to the methyl group. It appears that initially the β electron density moves to the cobalt only to remove the spin polarization, and after that point, the picture is similar to that noticed for the B3LYP. In both cases, when the cleavage is completed, the spin density is localized essentially on the carbon, with practically no spin density on the cobalt and corrin.

The spin density changes shown in Figures 7 and 8 confirm the observation based on the potential energy curves, that the mechanism of oxidative cleavage is much simpler than the reductive cleavage,[22,23] because in the former only one electronic state is involved, while more electronic states, which involve π^* and σ^* orbitals, play a significant role in the latter.

3.6. CASSCF/MC-XQDPT2 Analysis of the 1e-Ox MeCbl. Taking into account that the BP86 functional gives the spin density that is evenly distributed between Co and the corrin ligand, whereas B3LYP shows that the spin density is shifted more toward corrin, we turned our attention to a higher-level *ab initio* method. We used the modified version of the second-order multiconfigurational quasi-degenerate perturbation theory (MC-QDPT2) of Nakano,[60] abbreviated as a MC-XQDPT2, employing complete active space self-consistent field (CASSCF) reference wave functions.

In CASSCF-based multireference computations, one of the most challenging steps is the selection of an active space, especially for large molecules comprised of transition metals and tetrapyrrolic ligands such as corrin. In the case of MeCbl, the process of selecting active orbitals was advocated by the active spaces that were previously employed in cobalamin's derivatives,[69−71] which were found to be the most appropriate for the excited state benchmark calculations and the cleavage of the Co−C bond. The active space includes 3d-type orbitals (d_{xz}, d_{yz}, $d_{x^2-y^2}$) of cobalt, π-type orbitals of the corrin ring, as well as the $\sigma(d_{z^2})$ orbital associated with the axial bonding σ(Co−C). In addition, the 4d orbitals of the cobalt as well as lowest unoccupied π^* corrin orbitals were also included in the correlating orbitals in order to account for the double-shell effect.[72] As a result, the final active space of the 1e-Ox MeCbl was comprised of four occupied d orbitals of cobalt, two occupied π-type orbitals of corrin, and six corresponding correlating orbitals (virtual), which subsequently gives 11 active electrons distributed in 12 active orbitals (Figure 9). The possibility of several other active spaces has also been tested; however, the CASSCF(11,12) seems to be the appropriate active space for the analysis of electronic structure of the 1e-Ox MeCbl.

To obtain an accurate description of the low-lying excited states along with the ground state, CASSCF itself is not sufficient because it does not account for the dynamical correlation effects. Therefore, in order to include the dynamical correlation, we carried out state-average SA-CASSCF calculations followed by the second order perturbation theory (QDPT2). The SA-CASSCF/MC-XQDPT2 calculations reveal that the ground state wave function of the 1e-Ox MeCbl has multireference character with three major configuration state

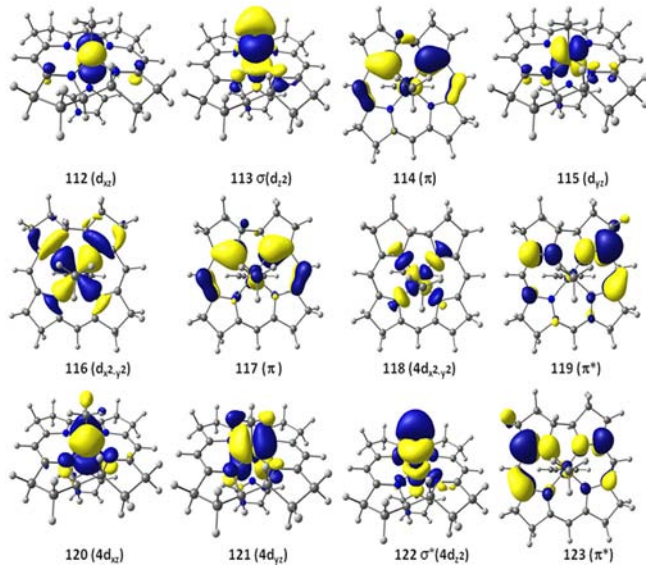

Figure 9. Active space orbitals of 1e-Ox MeCbl used in CASSCF (11,12) calculations.

functions (CSFs), as shown in Table 4. Notably, the single electron is located on d_{yz} of Co and the π orbital of corrin with 49% and 26% weight contributions, respectively. The ground state wave function also has minor contributions (10%) from the quartet state, which corresponds to electron transfer from a σ(Co−C) bond to a σ^*(Co−C) bond. This partial depopulation of the σ(Co−C) orbital can considerably reduce the strength of the Co−C bond and is one of the main reasons for the observed lowering of dissociation energy in DFT calculations. In addition, SA-CASSCF/MC-XQDPT2 calculations demonstrate that the first excited state is nearly degenerate with respect to ground state and has very low excited state energy (0.22 eV). The corresponding wave function also shows the same type of mulitreference character as that of the doublet ground state but the unpaired electron is mainly localized on d_{xz} and π orbital of the corrin (Table 4).

Furthermore, we verified the effect of water solvent on the low-lying electronic state using CASSCF/MC-XQDPT2 calculations, which are embedded in the polarized continuum model (PCM) as implemented in the firefly/PC-GAMMES suite of programs.[61] The presence of the solvent environment does not alter the multireference character of the ground state as well as the excited states. As we have discussed above, there are two major configurations (CSF_1 and CSF_2), the first one which is Co(IV) corrin with 49% weight while the second one is the Co(III) π-cation corrin radical with 26% weight (Table 4). However, the contribution of these two configurations in the first excited state is different than in the ground state: the weight percentage of Co(IV) corrin is increased up to 65%, whereas the Co(III) π-cation corrin radical character is reduced to 10%. In addition, it is important to mention that the calculated energies of the low-lying excited states are very similar to the those resulting from the gas phase calculations, but the solvent environment decreases the energy of the first and the second excited states by 0.003 and 0.005 eV, respectively (Table 4), while it increases the energy of the third excited state by 0.04 eV.

The local environment of the corrin under D_{4h} pseudo-symmetry was considered to analyze interactions between low-lying electronic states from SA-CASSCF/QDPT2 calculations.

dx.doi.org/10.1021/ic3013443 | *Inorg. Chem.* 2013, 52, 1762−1771

Table 4. Composition of CASSCF/MC-XQDPT2 Wave Function of 1e-Ox MeCbl in terms of Major Configurations State Functions (CSFs) Computed for First Three Excited States[a]

state	$E^{b}_{\text{MC-XQDPT2}}$	CSF_1 (weight%)	CSF_2 (weight%)	CSF_3 (weight%)
0	0.000 (0.000)	222122000000 (49)	221222000000 (26)	202122000020 (10)
1	0.228 (0.225)	122222000000 (65)	222221000000 (10)	102222000020 (9)
2	1.837 (1.832)	212222000000 (81)	202222000010 (6)	
3	3.807 (3.811)	122122000010 (32)	121222000010 (17)	112122000020 (15)

[a]The active space occupations are described by 11 active electrons in 12 active orbitals, where 0 means unoccupied, 1 means singly occupied, and 2 means doubly occupied. The active space orbitals are shown in Figure 9. [b]The MC-XQDPT2 energies are in eV, and energy values calculated in the water solvent are shown in parentheses.

Because four Co−N(corrin) bonds in corrin are nonequivalent, there should be a distortion of cobalt 3d orbitals and π-type orbitals of the corrin ligand. The Co(III) ion has a d^6 configuration under pseudo-D_{4h} symmetry that contains three highest occupied molecular orbitals (HOMO) of e_g (d_{xz} and d_{yz}) and a_{1g} (d_{z^2}) symmetry and two unoccupied d orbitals of b_{1g} and b_{2g} symmetry. When an electron is removed from the MeCbl, 3d orbitals of the Co are strongly mixed with an a_{2u}/a_{1u} symmetry based π-type HOMO orbital of the corrin. The actual picture turns out to be more complicated upon the removal of an electron because the d_{yz} and d_{xz} orbitals are nearly degenerate, the resulting electronic configuration becomes unstable, and the molecular system experiences a pseudo-Jahn−Teller (pJT) effect. This can produce more than one electronic configuration and a near-degeneracy between the ground state and low lying excited states, as 3d orbitals of Co metal are degenerate and mix at the same time with π-corrin orbitals. According to SA-CASSCF/MC-XQDPT2 calculations of the 1e-Ox MeCbl, the unpaired electron is predominantly localized on d_{yz} and corrin π in the ground state, while in the first excited state (pseudo-ground state), it is located on d_{xz}/d_{z^2} and corrin π orbital. It has been demonstrated by Bersuker[73,74] that a low energy gap between vibronically coupled electronic states is the major consequence of the pJT effect. The pJT effect can only be demonstrated with multiconfigurational methods such as CASSCF, as they account for the nondynamical (near-degeneracy) correlation effects,[75] which can lead to a nonadiabatic coupling between the electronic states. Indeed, the absence of the pJT effect in DFT seems to be logical for the 1e-Ox MeCbl because the conventional Kohn−Sham DFT method does not include nondynamical correlation effects. The presence of the pJT effect leads to a significant change in electronic properties of the open-shell system, i.e., cation radicals.[76,77] Note that the theory of the pJT effect is well pronounced for highly symmetrical systems (i.e., metalloporphyrin) because it involves the coupling of the symmetrical states.[78−80]

It can be concluded that the multireference CASSCF/MC-XQDPT2 method provides a better picture of the single electron distribution due to several effects that the conventional DFT method cannot account for. The CASSCF calculations also suggest that the single electron is not located at the Co−C bond in the ground state, which is in agreement with the DFT approach. The CASSCF/MC-XQDPT2 computations, which comprise a wave function based method, seem to resolve the confusion about the location of the unpaired electron caused by differences observed with different density functionals. These high-level computations indicate that a single electron resides both on the cobalt and on the π-type corrin orbitals, which is qualitatively consistent with the spin polarization obtained from the BP86 functional. As a consequence, the oxidized species of MeCbl species is better described by an admixture of the π-cation corrin radical and the Co(III)/Co(IV) oxidation state.

4. SUMMARY AND CONCLUSIONS

The present theoretical study is among the first in which DFT and CASSCF/MC-XQDPT2 calculations have been employed to investigate the electronic and structural properties of the one-electron-oxidized cobalt corrinoids. In particular, the DFT/BP86 and the DFT/B3LYP levels of theory have been used to explore the mechanism of the Co−C oxidative bond cleavage in the MeCbl cofactor. The most appealing result of the present contribution is significant lowering of the dissociation energy (~35%), which might be due to partial depopulation of the Co−C σ orbital.

The employed DFT functionals provide a different description regarding the spin density distribution in the 1e-Ox species: the BP86 demonstrates that spin density is evenly distributed between Co and corrin while it shifts more toward the corrin ring in the case of the B3LYP functional, which is more in line with the corrin π radical and Co(III) oxidation state. It is important to note that the DFT study only supports the formation and involvement of the Co(IV) oxidation state if the results of the BP86 functional are considered. However, the state-of-the-art higher level CASSCF/MC-XQDPT2 computations also advocate the formation of the Co(IV) oxidation state of the 1e-Ox MeCbl with some contribution from corrin π-radical Co(III) character. In addition, the CASSCF/MC-XQDPT2 calculations confirm that the unpaired electron is delocalized on different active orbitals (d orbital of Co and corrin π) where a strong mixing of electronic states has been observed upon the inclusion of a nondynamical correlation effect. A near-degeneracy between the ground and the first excited state is the result of a pseudo-Jahn−Teller (pJT) effect, as it is usually pronounced for paramagnetic species. Consequently, the oxidized species of MeCbl can be adequately described as a mixed corrin π-radical Co(III)/Co(IV) complexes.

It is important to mention that the change in Co−C bond in the 1e-Ox model of MeCbl as compared to the neutral complex is opposite the observations made for the 1e-Red MeCbl analogue as it is exemplified for data based on the BP86 functional (Table 1). The Co−C bond slightly lengthens upon electron removal while it shortens upon electron addition. These contrary changes can be attributed to the fact that for the 1e-Red species the electron is almost entirely located on the corrin ligand while removal of the electron partially induces the Co(IV) character. These theoretical results are further supported by the experimental study of Fanchiang et al., which suggested that the oxidative cleavage mechanism is the plausible pathway for the methyl transfer reactions between MeCbl and diaquo-Co(III)cobinamide.[38] At present the most

dx.doi.org/10.1021/ic3013443 | Inorg. Chem. 2013, 52, 1762−1771

challenging problem is the potential involvement of the oxidized forms of cobalamins and their respective oxidative cleavage mechanism in B_{12}-catalyzed enzymatic reactions, which has yet to be confirmed.

Furthermore, the DFT computations suggest that the Pyr-[Co(Por)]$^{\bullet}$-Me^{+} species are Co(III) ligand π radicals rather than the Co(IV) complexes, which is in agreement with experimental findings by Fukuzumi et al., for the Pyr-[Co(TPP)]$^{\bullet}$-Me^{+}.[35] However, the Co(III)/Co(IV) balance is quite delicate and could be shifted even by removal of the *meso* phenyls in the model structure. The calculated Co−C bonds are shorter in B-[Co(Por)]$^{\bullet}$-Me^{+} than that of the 1e-Ox MeCbl. This observation together with a comparison of the composition of the SOMOs, and the spin distribution between Co and the equatorial ligand, shows that the corrin complex has a more Co(IV) character than its porphine analogues, which seems to facilitate the bond cleavage. Thus, the corrin ligand shows some preference for the oxidative Co−C bond cleavage, as compared to porphyrin. This implies that one electron oxidation of MeCbl has a considerable weakening effect on the Co−C bond, although this effect is not as strong as in the case of one electron reduction.

The calculated DFT potential energy curves show that only one electronic state is involved in the bond rupture of the 1e-Ox complex of MeCbl, while in the 1e-Red species, a considerable electronic rearrangement occurs during state crossing. The investigation of the Co−C bond dissociation process followed by changes in spin distribution is troublesome, when BP86 is considered, which is due to the predicted strong spin polarization, whereas the hybrid B3LYP functional gives a quite clear picture for the β electron transfer from the Co−C bond to the equatorial corrin ligand with the cobalt atom playing the role of a conductor. Thus, the 1e-Ox MeCbl and B-[Co(Por)]$^{\bullet}$-Me^{+} are other examples of paramagnetic metal complexes containing a noninnocent ligand that cannot be successfully analyzed in terms of total spin distribution, unless spin polarization is accounted for.

■ ASSOCIATED CONTENT

Supporting Information

Pictures of essential molecular orbitals for the 1e-Ox MeCbl determined at different DFT functionals, spin density at various Co−C bond lengths for the 1e-Ox MeCbl, relevant energetic and geometrical parameters of the neutral and 1e-Ox MeCbl optimized at different functionals, and orbital energies (α and β) and composition of the 1e-Ox MeCbl system molecular orbitals determined using different DFT functionals. This material is available free of charge via the Internet at http://pubs.acs.org.

■ AUTHOR INFORMATION

Corresponding Author

*Tel.: (502) 852-6609. Fax: (502) 852-8149. E-mail: pawel@louisville.edu.

Notes

The authors declare no competing financial interest.

■ ACKNOWLEDGMENTS

N.K. and P.M.K. acknowledge the computer support and assistance provided by Cardinal Research Cluster Center at the University of Louisville. The financial support from Polish Ministry of Science & Higher Education Grant No. N204 163236 for W.G. is gratefully acknowledged.

■ REFERENCES

(1) Dolphin, D. *B12*; Wiley-Interscience: New York, 1982.
(2) Banerjee, R. *Chem. Biol.* **1997**, *4*, 175.
(3) Ludwig, M. L.; Matthews, R. G. *Annu. Rev. Biochem.* **1997**, *66*, 269.
(4) Banerjee, R. *In Chemistry and Biochemistry of B12*; John Wiley & Sons: New York, 1999.
(5) Toraya, T. *Cell. Mol. Life Sci.* **2000**, *57*, 106.
(6) Ragsdale, S. W. *In Chemistry and Biochemistry of B12*; John Wiley & Sons: New York, 1999.
(7) Sauer, K. T. *In Chemistry and Biochemistry of B12*; John Wiley & Sons: New York, 1999.
(8) Lexa, D.; Saveant, J. M. *J. Am. Chem. Soc.* **1978**, *100*, 3220.
(9) Lexa, D.; Saveant, J. M. *Acc. Chem. Res.* **1983**, *16*, 235.
(10) Kim, M. H.; Birke, R. L. *J. Electroanal. Chem. Interfacial Electrochem.* **1983**, *144*, 331.
(11) Matthews, R. G. *Acc. Chem. Res.* **2001**, *34*, 681.
(12) Birke, R. L.; Huang, Q.; Spataru, T.; Gosser, D. K., Jr. *J. Am. Chem. Soc.* **2006**, *128*, 1922.
(13) Spataru, T.; Birke, R. L. *J. Electroanal. Chem.* **2006**, *593*, 74.
(14) Corrinoids are a family of cofactors with structures similar to cobalamin. In corrinoids, the dimethylbenzimidazole (DBI) that is present in cobalamin is modified or replaced by an alternate ligand.
(15) Costa, G.; Puxeddu, A.; Reisenhofer, E. *J. Chem. Soc., Dalton Trans.* **1972**, 1519.
(16) Elliott, C. M.; Hershenhart, E.; Finke, R. G.; Smith, B. L. *J. Am. Chem. Soc.* **1981**, *103*, 5558.
(17) Costa, G.; Puxeddu, A.; Tavagnacco, C. *J. Organomet. Chem.* **1985**, *296*, 161.
(18) Guilard, R.; Kadish, K. M. *Chem. Rev.* **1988**, *88*, 1121.
(19) Kadish, K. M.; Han, B. C.; Endo, A. *Inorg. Chem.* **1991**, *30*, 4502.
(20) Galezowski, W. *Inorg. Chem.* **2005**, *44*, 5483.
(21) Pratt, D. A.; van der Donk, W. A. *J. Am. Chem. Soc.* **2005**, *127*, 384.
(22) Kozlowski, P. M.; Kuta, J.; Galezowski, W. *J. Phys. Chem. B* **2007**, *111*, 7638.
(23) Galezowski, W.; Kuta, J.; Kozlowski, P. M. *J. Phys. Chem. B* **2008**, *112*, 3177.
(24) Alfonso-Prieto, M.; Biarnes, X.; Kumar, M.; Rovira, C.; Kozlowski, P. M. *J. Phys. Chem. B* **2010**, *114*, 12965.
(25) Agnes, G.; Hill, H. A. O.; Pratt, J. M.; Ridsdale, S. C.; Kennedy, F. S.; Williams, R. J. P. *Biochim. Biophys. Acta* **1971**, *252*, 207.
(26) Vol'pin, M. E.; Levitin, I. Y.; Sigan, A. L.; Nikitaev, A. T. *J. Organomet. Chem.* **1985**, *279*, 263.
(27) Chopra, M.; Hun, T. S. M.; Leung, W.-H.; Yu, N.-T. *Inorg. Chem.* **1995**, *34*, 5973.
(28) Rubinson, K. A.; Itabashi, E.; Mark, H. B. *Inorg. Chem.* **1982**, *21*, 3571.
(29) Nahor, G. S.; Neta, P.; Hambright, P.; Robinson, L. R. *J. Phys. Chem.* **1991**, *95*, 4415.
(30) Guldi, D. M.; Field, J.; Grodkowski, J.; Neta, P.; Vogel, E. *J. Phys. Chem.* **1996**, *100*, 13609.
(31) Halpern, J.; Chan, M. S.; Hanson, J.; Roche, T. S.; Topich, J. A. *J. Am. Chem. Soc.* **1975**, *97*, 1606.
(32) Halpern, J.; Topich, J.; Zamaraev, K. I. *Inorg. Chim. Acta* **1976**, *20*, L21.
(33) Topich, J.; Halpern, J. *Inorg. Chem.* **1979**, *18*, 1339.
(34) Methylcobaloxime = methyl bis(dimethylglyoximato)Co(III).
(35) Fukuzumi, S.; Miyamoto, K.; Suenobu, T.; Caemelbecke, E. V.; Kadish, K. M. *J. Am. Chem. Soc.* **1998**, *120*, 2880.
(36) Dolphin, D.; Halko, D. J.; Johnson, E. *Inorg. Chem.* **1981**, *20*, 4348.
(37) Ohkubo, K.; Fukuzumi, S. *J. Phys. Chem. A* **2005**, *109*, 1105.
(38) Fanchiang, Y. T.; Bratt, G. T.; Hogenkamp, H. P. *Proc. Natl. Acad. Sci. U. S. A.* **1984**, *81*, 2698.

(39) Tamblyn, W. H.; Klingler, R. J.; Hwang, W. S.; Kochi, J. K. *J. Am. Chem. Soc.* **1981**, *103*, 3161.
(40) Fanchiang, Y. T. *Inorg. Chem.* **1982**, *21*, 2344.
(41) Fanchiang, Y. T. *Inorg. Chem.* **1983**, *22*, 1693.
(42) Fanchiang, Y. T. *Organometallics* **1983**, *2*, 121.
(43) Fanchiang, Y. T. *Inorg. Chem.* **1984**, *23*, 3983.
(44) Drennan, C. L.; Huang, S.; Drummond, J. T.; Matthews, R. G.; Lidwig, M. L. *Science* **1994**, *266*, 1669.
(45) Kuta, J.; Patchkovskii, S.; Zgierski, M. Z.; Kozlowski, P. M. *J. Comput. Chem.* **2006**, *27*, 1429.
(46) Rovira, C.; Kozlowski, P. M. *J. Phys. Chem. B* **2007**, *111*, 3251.
(47) Kozlowski, P. M.; Kamachi, T.; Toraya, T.; Yoshizawa, K. *Angew. Chem., Int. Ed.* **2007**, *46*, 980.
(48) Dölker, N.; Morreale, A.; Maseras, F. *J. Biol. Inorg. Chem.* **2005**, *10*, 509.
(49) Jensen, K. P.; Ryde, U. *ChemBioChem* **2003**, *4*, 413.
(50) Becke, A. D. *J. Chem. Phys.* **1986**, *84*, 4524.
(51) Perdew, J. P. *Phys. Rev. B* **1986**, *33*, 8822.
(52) Frisch, M. J.; Trucks, G. W.; Schlegel, H. B.; Scuseria, G. E.; Robb, M. A.; Cheeseman, J. R.; Montgomery, J. A., Jr.; Vreven, T.; Kudin, K. N.; Burant, J. C.; Millam, J. M.; Iyengar, S. S.; Tomasi, J.; Barone, V.; Mennucci, B.; Cossi, M.; Scalmani, G.; Rega, N.; Petersson, G. A.; Nakatsuji, H.; Hada, M.; Ehara, M.; Toyota, K.; Fukuda, R.; Hasegawa, J.; Ishida, M.; Nakajima, T.; Honda, Y.; Kitao, O.; Nakai, H.; Klene, M.; Li, X.; Knox, J. E.; Hratchian, H. P.; Cross, J. B.; Bakken, V.; Adamo, C.; Jaramillo, J.; Gomperts, R.; Stratmann, R. E.; Yazyev, O.; Austin, A. J.; Cammi, R.; Pomelli, C.; Ochterski, J. W.; Ayala, P. Y.; Morokuma, K.; Voth, G. A.; Salvador, P.; Dannenberg, J. J.; Zakrzewski, V. G.; Dapprich, S.; Daniels, A. D.; Strain, M. C.; Farkas, O.; Malick, D. K.; Rabuck, A. D.; Raghavachari, K.; Foresman, J. B.; Ortiz, J. V.; Cui, Q.; Baboul, A. G.; Clifford, S.; Cioslowski, J.; Stefanov, B. B.; Liu, G.; Liashenko, A.; Piskorz, P.; Komaromi, I.; Martin, R. L.; Fox, D. J.; Keith, T.; Al-Laham, M. A.; Peng, C. Y.; Nanayakkara, A.; Challacombe, M.; Gill, P. M. W.; Johnson, B.; Chen, W.; Wong, M. W.; Gonzalez, C.; Pople, J. A. *Gaussian 03*, revision C.02; Gaussian, Inc.: Wallingford, CT, 2004.
(53) Jaworska, M. *Chem. Phys.* **2007**, *332*, 203.
(54) Jensen, K. P. *J. Phys. Chem. B* **2005**, *109*, 10505.
(55) Kumar, N.; Alfonso-Prieto, M.; Rovira, C.; Lodowski, P.; Jaworska, M.; Kozlowski, P. M. *J. Chem. Theory Comput.* **2011**, *7*, 1541.
(56) Perdew, J. P.; Burke, K.; Ernzerhof, M. *Phys. Rev. Lett.* **1996**, *77*, 3865.
(57) Jensen, K. P.; Ryde, U. *J. Phys. Chem. A* **2003**, *107*, 7539.
(58) Ruiz, E.; Cirera, J.; Alvarez, S. *Coord. Chem. Rev.* **2005**, *249*, 2649.
(59) Becke, A. D. *J. Chem. Phys.* **1993**, *98*, 5648.
(60) Nakano, H. *J. Chem. Phys.* **1993**, *99*, 7983.
(61) Granovsky, A. A. PC GAMESS/Firefly version 7.1.G. www.http://classic.chem.msu.su/gran/gamess/index.html.
(62) Randaccio, L.; Furlan, M.; Geremia, S.; Slouf, M.; Srnova, I.; Toffoli, D. *Inorg. Chem.* **2000**, *39*, 3403.
(63) Strain orbital.
(64) Remenyi, C.; Kaupp, M. *J. Am. Chem. Soc.* **2005**, *127*, 11399.
(65) Martin, B. D.; Finke, R. G. *J. Am. Chem. Soc.* **1992**, *114*, 585.
(66) Hung, R. R.; Grabowski, J. J. *J. Am. Chem. Soc.* **1999**, *121*, 1359.
(67) Dölker, N.; Maseras, F.; Lledós, A. *J. Phys. Chem. B* **2002**, *107*, 306.
(68) Dölker, N.; Maseras, F.; Lledós, A. *J. Phys. Chem. B* **2001**, *105*, 7564.
(69) Kornobis, K.; Kumar, N.; Wong, B. M.; Lodowski, P.; Jaworska, M.; Andruniow, T.; Ruud, K.; Kozlowski, P. M. *J. Phys. Chem. A* **2011**, *115*, 1280.
(70) Kumar, N.; Jaworska, M.; Lodowski, P.; Kumar, M.; Kozlowski, P. M. *J. Phys. Chem. B* **2011**, *115*, 6722.
(71) Kornobis, K.; Kumar, N.; Wong, B. M.; Jaworska, M.; Lodowski, P.; Kozlowski, P. M. *J. Comput. Chem.* **2013**. In press (DOI: 10.1002/jcc.23204).
(72) Roos, B. O.; Lindh, R.; Malmqvist, P.-A.; Veryazov, V.; Widmark, P.-O. *J. Phys. Chem. A* **2005**, *109*, 6575.
(73) Bersuker, I. B. *J. Comput. Chem.* **1997**, *18*, 260.
(74) Bersuker, I. B. *Chem. Rev.* **2001**, *101*, 1067.
(75) Andersson, K.; Malmqvist, P.-A.; Roos, B. O. *J. Chem. Phys.* **1992**, *96*, 1218.
(76) Vangberg, T.; Lie, R.; Ghosh, A. *J. Am. Chem. Soc.* **2002**, *124*, 8122.
(77) Williams, F. *Radiat. Phys. Chem.* **2003**, *67*, 211.
(78) Prendergast, K.; Spiro, T. G. *J. Phys. Chem.* **1991**, *95*, 9728.
(79) Hirao, H.; Shaik, S.; Kozlowski, P. M. *J. Phys. Chem. A* **2006**, *110*, 6091.
(80) Yoshizawa, K.; Nakayama, T.; Kamachi, T.; Kozlowski, P. M. *J. Phys. Chem. A* **2007**, *111*, 852.